

# HCl-Based Hydrothermal Etching Strategy toward Fluoride-Free MXenes

Changda Wang, Hongwei Shou, Shuangming Chen, Shiqiang Wei, Yunxiang Lin, Pengjun Zhang, Zhanfeng Liu, Kefu Zhu, Xin Guo, Xiaojun Wu, Pulickel M. Ajayan,\* and Li Song\*

Due to their ultrathin layered structure and rich elemental variety, MXenes are emerging as a promising electrode candidate in energy generation and storage. MXenes are generally synthesized via hazardous fluoride-containing reagents from robust MAX materials, unfortunately resulting in plenty of inert fluoride functional groups on the surface that noticeably decline their performance. Density functional theory calculations are used to show the etching feasibility of hydrochloric acid (HCl) on various MAX phases. Based on this theoretical guidance, fluoride-free Mo<sub>2</sub>C MXenes with high efficiency about 98% are experimentally demonstrated. The Mo<sub>2</sub>C electrodes produced by this process exhibit high electrochemical performance in supercapacitors and sodium-ion batteries owing to the chosen surface functional groups created via the HCl etch process. This strategy enables the development of fluoride-free MXenes and opens a new window to explore their potential in energy-storage applications.

## 1. Introduction

2D layered MXenes derived from transition metal carbides, nitrides, or carbonitrides have attracted numerous attention owing to their unique structure, electronic, and mechanical properties in various fields.<sup>[1,2]</sup> MXenes with a general formula of M<sub>n+1</sub>X<sub>n</sub>T<sub>x</sub> (*n* = 1–4) are usually obtained by removing “A” layers from the corresponding MAX phases (generally, M

is early transition metal, A is an element of Al, Si, Sn, or Ga, X is carbon and/or nitrogen), where T<sub>x</sub> stands for terminations such as –O, –F, –Cl, etc.<sup>[2]</sup> owing to the immunity of most MAX phases to common inorganic acids such as HCl or H<sub>2</sub>SO<sub>4</sub> in traditional cognition, the initial and universal strategy for selectively removing “A” layer is chemical etching by aqueous HF benefited from the much weaker metallic M–A bonds compared with covalent M–X bonds.<sup>[3]</sup> However, because of the high toxicity to human body and danger to handle for HF reagent, an essential and much more moderate approach was emerged based on mixed compounds of fluoride salts (LiF, NaF, etc.) and acids (HCl, H<sub>2</sub>SO<sub>4</sub>).<sup>[4]</sup> Even though, the F-involved reagents often lead in much –F termination on MXenes inevitably,

impacting the electronic conductivity,<sup>[5]</sup> surface adjustability,<sup>[6]</sup> and electrochemical property as potential electrodes in supercapacitors and batteries.<sup>[7]</sup> Therefore, new synthesis strategies of fluoride-free MXenes are imperative to adjust their performance and extend the 2D MXenes.


So far, great efforts and several methods have been implemented to synthesize fluoride-free MXenes from MAX with “Al” layers. In brief, alkali including KOH and NaOH with high temperature and concentration were used to extract the Al layers especially for Ti<sub>3</sub>AlC<sub>2</sub> owing to the strong binding ability of OH<sup>–</sup> with Al elements.<sup>[8]</sup> Electrochemical etching process was another practicable approach to selectively remove Al layers in chloride-containing electrolytes by controlling the etching time and imposed voltage owing to the strong binding ability of Cl<sup>–</sup> with Al elements.<sup>[9]</sup> The route of using Lewis acidic molten salts was also proposed and generalized to prepare fluoride-free MXenes by adjusting MAX precursors with different Lewis acid salts under high temperature.<sup>[10]</sup> Nonetheless, the fully controlled etching of specific MAX is still big challenge (such as Mo<sub>2</sub>Ga<sub>2</sub>C<sup>[11]</sup> V<sub>2</sub>AlC, and Cr<sub>2</sub>AlC<sup>[12]</sup>), and F-containing reagents are inevitable for the preparation of Mo<sub>2</sub>C MXenes with high quality and large scale.<sup>[13–16]</sup> Thus, it is highly desirable to develop new efficient synthesis route for fluoride-free MXenes to further promote MXene’s high potentials.

Inspired from the strong binding capability of OH<sup>–</sup>/Cl<sup>–</sup> and “A” elements, various MAX materials with Al/Ga layers could be in principle etched by sole hydrochloric acid solution with

Dr. C. Wang, H. Shou, Dr. S. Chen, S. Wei, Y. Lin, P. Zhang, Z. Liu, K. Zhu, X. Guo, Prof. L. Song  
National Synchrotron Radiation Laboratory  
CAS Center for Excellence in Nanoscience  
University of Science and Technology of China  
Hefei, Anhui 230029, P. R. China  
E-mail: song2012@ustc.edu.cn

Prof. X. Wu  
School of Chemistry and Material Sciences  
University of Science and Technology of China  
Hefei, Anhui 230029, P. R. China

Prof. P. M. Ajayan  
Department of Materials Science and NanoEngineering  
Rice University  
Houston, TX 77005, USA  
E-mail: pma2@rice.edu

 The ORCID identification number(s) for the author(s) of this article can be found under <https://doi.org/10.1002/adma.202101015>.

DOI: 10.1002/adma.202101015

appropriate external power (like the thermal-assisted E-etching method<sup>[12]</sup>) by forming soluble  $\text{AlCl}_3$  and  $\text{GaCl}_3$ . Therefore, we firstly use the first-principle calculations to simulate the feasibility of various MAX materials with Al and Ga interlayer elements, predict the decisive etching conditions of temperature and pressure (T&P), and reveal the mystery of selective etching of MAX phases via HCl. Afterward, a simple and controllable HCl-hydrothermal etching method is experimentally proposed for various MAX materials including  $\text{Mo}_2\text{Ga}_2\text{C}$  and  $\text{Cr}_2\text{AlC}$ . The as-prepared fluoride-free  $\text{Mo}_2\text{CT}_x$  with high quality only shows Cl- and O-containing terminations and displays different capacitive behavior compared with  $\text{Mo}_2\text{CT}_x$  MXenes which is synthesized via HF-etching method. The optimization conditions are also discussed for the future preparation of different fluoride-free MXenes, which may greatly improve the efficiency compared with conventional trial-and-error method with uncertainty and heavy workload.

## 2. Results and Discussion

### 2.1. Density Functional Theory (DFT) Prediction of Hydrothermal Etching via HCl

Based on the first-principle calculations, **Figure 1** reveals simulated feasibility of etching in HCl for various MAX materials with Al and Ga interlayer elements. The fundamental principle is that the chemical potential of “A” in products of  $\text{AlCl}_3$  ( $A = \text{Al}, \text{Ga}$ ) should be lower than that of “A” in MAX, i.e.,  $\mu_A(\text{AlCl}_3) < \mu_A(\text{MAX})$ . Further, the chemical potential of A in solid MAX is set as constant and the chemical potential of A in  $\text{AlCl}_3$  can be regulated by HCl and  $\text{H}_2$  which is extraordinarily sensitive to temperature and pressure. Figure 1a shows the mapping of simulated chemical potential of Al in  $\text{AlCl}_3$  ( $\mu_{\text{Al}}(\text{AlCl}_3)$ ) influenced by T&P.<sup>[17]</sup>  $\mu_{\text{Al}}(\text{AlCl}_3)$  will gradually decrease with the reduction of both temperature and pressure, which is conducive to the etching of MAX phases in thermodynamics. However, in kinetics, higher temperature will improve the etching efficiency on practical experiments. Therefore, we

studied the reaction-limiting temperature ( $T_{\text{RL}}$ )<sup>[18]</sup> based on pressure during etching process for different MAX materials (the dotted lines in Figure 1a). According to our calculations,  $\text{TiVAAlC}$ ,  $\text{Nb}_2\text{AlC}$ ,  $\text{Ta}_2\text{AlC}$ ,  $\text{V}_2\text{AlC}$ , and  $\text{Cr}_2\text{AlC}$  can be successfully etched into corresponding MXenes ( $\text{TiVCT}_x$ ,  $\text{Nb}_2\text{CT}_x$ ,  $\text{Ta}_2\text{CT}_x$ ,  $\text{V}_2\text{CT}_x$ , and  $\text{Cr}_2\text{CT}_x$ ) in HCl solution and the  $T_{\text{RL}}$  are 325, 400, 410, 420, and 750 K, respectively, under fixed pressure of 1 atm. Moreover, the calculated  $T_{\text{RL}}$  slightly decrease with the rise of pressure. It is predicted that  $\text{Cr}_2\text{AlC}$  could be the most favorable material to be etched, which is experimentally proved in Figures S1 and S2 (Supporting Information). Contrarily, the chemical potentials of Al in  $\text{V}_4\text{AlC}_3$ ,  $\text{Nb}_4\text{AlC}_3$ ,  $\text{Ta}_4\text{AlC}_3$ ,  $\text{Ti}_2\text{AlN}$ ,  $\text{Ti}_4\text{AlN}_3$ ,  $\text{Ti}_3\text{AlC}_2$ ,  $\text{Nb}_3\text{AlC}_2$ , and  $\text{Ti}_5\text{Al}_2\text{C}_3$  are always lower than  $\mu_{\text{Al}}(\text{AlCl}_3)$ , indicating the impossibility of their etching in HCl (Table S1, Supporting Information). Except “Al” based MAX phases, the mapping of chemical potential of Ga in  $\text{GaCl}_3$  ( $\mu_{\text{Ga}}(\text{GaCl}_3)$ ) and the line of  $\Delta G = 0$  for MAX materials with Ga interlayer atoms is also exhibited in Figure 1b. It is predicted that  $\text{Cr}_2\text{GaC}$ ,  $\text{Mo}_2\text{GaC}$ ,  $\text{Mo}_2\text{Ga}_2\text{C}$ , and  $\text{Mn}_2\text{GaC}$  could be successfully etched into corresponding MXenes ( $\text{Cr}_2\text{CT}_x$ ,  $\text{Mo}_2\text{CT}_x$ ,  $\text{Mo}_2\text{CT}_x$ , and  $\text{Mn}_2\text{CT}_x$ ) in HCl solution, and the  $T_{\text{RL}}$  at 1 atm are 385, 435, 455, and 485 K, respectively. Conversely,  $\text{Nb}_2\text{GaC}$ ,  $\text{Ta}_2\text{GaC}$ ,  $\text{Ti}_2\text{GaC}$ ,  $\text{Ti}_2\text{GaN}$ ,  $\text{Ti}_3\text{GaC}_2$ ,  $\text{Ti}_4\text{GaC}_3$ ,  $\text{V}_2\text{GaC}$ ,  $\text{V}_2\text{Ga}_2\text{C}$ , and  $\text{V}_2\text{GaN}$  are impossible to be etched in HCl owing to the lower chemical potential of Ga than  $\mu_{\text{Ga}}(\text{GaCl}_3)$  (Table S2, Supporting Information).

In brief, the above calculation results reveal that many MAX phases can be successfully etched in sole HCl solution by forming  $\text{AlCl}_3$  ( $A = \text{Al}, \text{Ga}$ ). Meanwhile, the pressure and temperature play a vital role during the etching process with a unique  $T_{\text{RL}}$ . Moreover, the comparison study of feasibility of HF etching strategy for various MAX phases based on Gibbs free energy is also studied via DFT, as shown in Figure S3 and Tables S1 and S2 (Supporting Information) which are certified in experiments.<sup>[3]</sup> Based on the instruction of DFT results, we proposed a simple and controllable hydrochloric acid assisted hydrothermal etching strategy with appropriate temperature and pressure for fluoride-free MXenes.

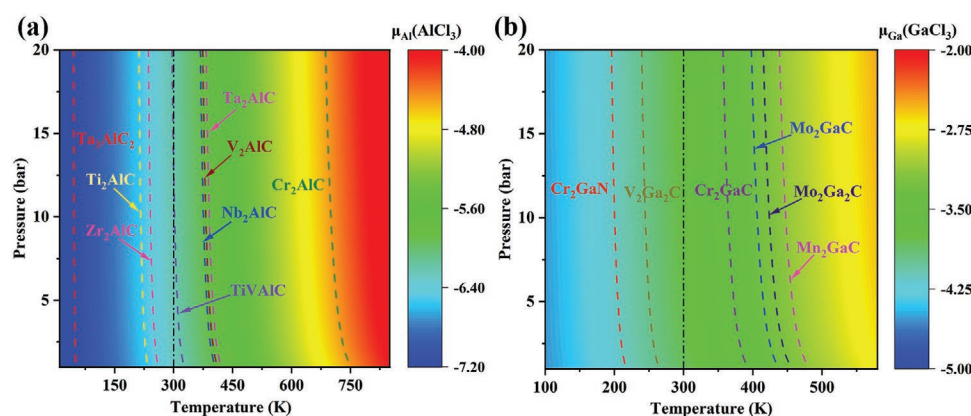


**Figure 1.** Feasibility of HCl-assisted hydrothermal etching strategy for various MAX phases. a) The mapping of chemical potential of Al in  $\text{AlCl}_3$  ( $\mu_{\text{Al}}(\text{AlCl}_3)$ ) influenced by temperature and pressure. The difference of Gibbs free energy ( $G$ ) determines the feasibility of etching. The dotted line indicates the  $\Delta G = 0$  ( $\Delta G = \mu_{\text{Al}}(\text{AlCl}_3) - \mu_{\text{Al}}(\text{MAX})$ ), left and right areas of dotted line indicate  $\Delta G < 0$  and  $\Delta G > 0$ , respectively. b) The mapping of chemical potential of Ga in  $\text{GaCl}_3$  ( $\mu_{\text{Ga}}(\text{GaCl}_3)$ ) influenced by temperature and pressure. The dotted line indicates the  $\Delta G = 0$  ( $\Delta G = \mu_{\text{Ga}}(\text{GaCl}_3) - \mu_{\text{Ga}}(\text{MAX})$ ), left and right areas of dotted line indicate  $\Delta G < 0$  and  $\Delta G > 0$ , respectively. The single point line stands for room temperature.

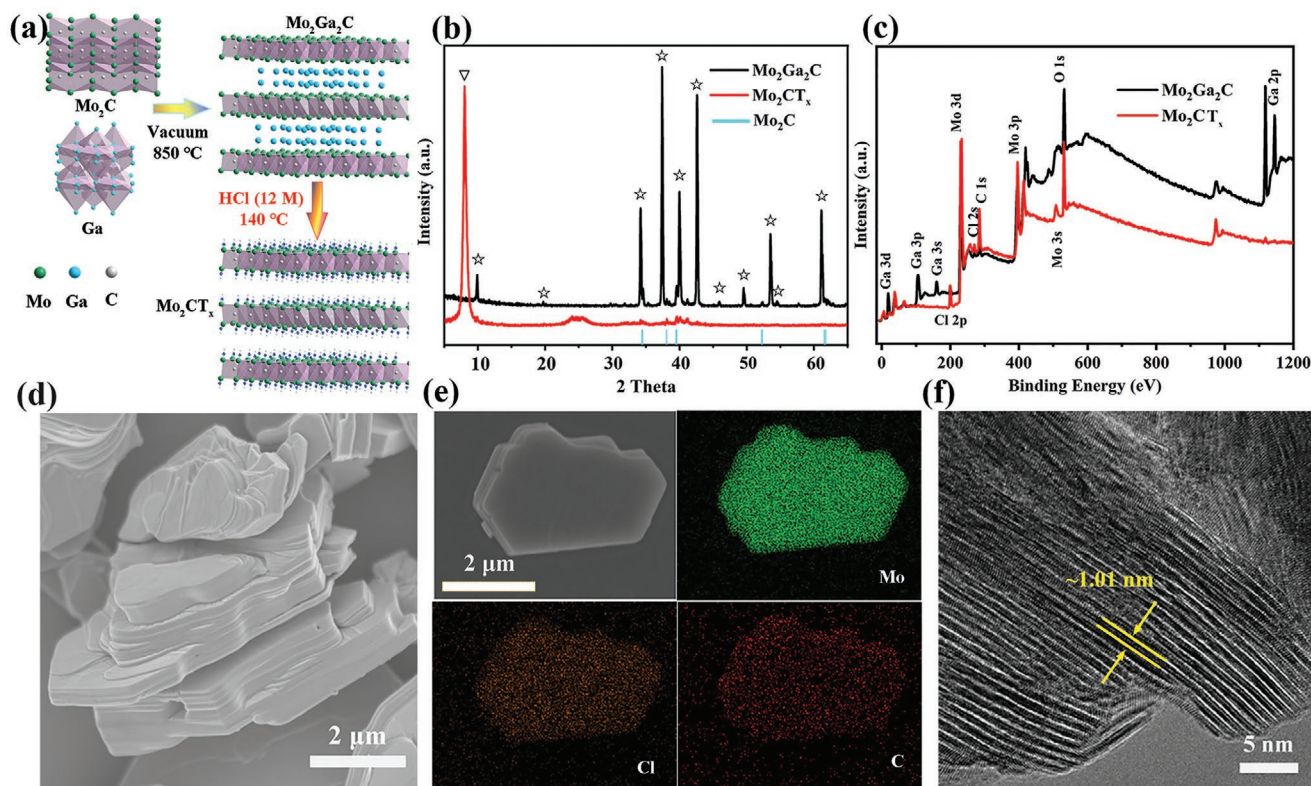


**Figure 2.** Fluoride-free Mo<sub>2</sub>CT<sub>x</sub> prepared by sole HCl-assisted hydrothermal etching strategy. a) Schematic illustration of the preparation procedure for fluoride-free Mo<sub>2</sub>CT<sub>x</sub>. b) X-ray diffraction patterns of Mo<sub>2</sub>Ga<sub>2</sub>C and Mo<sub>2</sub>CT<sub>x</sub> MXenes; the peaks marked with stars are the main diffraction peaks from Mo<sub>2</sub>Ga<sub>2</sub>C. c) XPS survey spectrum of Mo<sub>2</sub>Ga<sub>2</sub>C and Mo<sub>2</sub>CT<sub>x</sub> MXenes. d–f) SEM, elemental-mapping images (Mo, Cl, and C elements) (e), and HRTEM (f) of Mo<sub>2</sub>CT<sub>x</sub> MXenes, respectively.

## 2.2. Hydrothermal Etching of Mo<sub>2</sub>Ga<sub>2</sub>C via HCl

As a proof-of-concept demonstration, we select Mo<sub>2</sub>Ga<sub>2</sub>C as a typical MAX precursor to achieve fluoride-free Mo<sub>2</sub>C MXenes. Based on the above calculated feasibility results, a controllable hydrothermal reaction is developed with the assistance of HCl. The schematic procedure is shown in Figure 2a. Before the implementation of etching experiment, high-quality Mo<sub>2</sub>Ga<sub>2</sub>C is firstly synthesized via a two-stage vacuum sintering process.<sup>[19]</sup> The detailed synthesis process is shown in the Experimental Section. Then, Mo<sub>2</sub>Ga<sub>2</sub>C and concentrated HCl are put into autoclave with a Teflon liner to extract Ga atoms from the interlayers. Considering the significant effect of T&P on etching efficiency and  $T_{RL}$  from DFT results together with high production, the volume fraction of concentrated HCl in Teflon liner and temperature are set as 40% and 140 °C with pressure about 15 bar (Figure S4, Supporting Information). As expected, the Mo<sub>2</sub>CT<sub>x</sub> MXenes with high purity is finally obtained. The X-ray diffraction (XRD) results as shown in Figure 2b exhibit the high quality of Mo<sub>2</sub>Ga<sub>2</sub>C benefiting from the modified synthesis procedures. The main peaks located at 9.89°, 34.18°, 37.4°, 39.94°, 42.58°, 49.52°, 53.5°, and 61.1° are assigned to (002), (100), (103), (008), (105), (107), (108), and (110) diffractions, respectively. Moreover, there is little residue of unreacted commercial Mo<sub>2</sub>C impurity (PDF No. 77-0720). After removing Ga, the (002) peak marked with triangle shifts to lower angle around 8° and other diffraction peaks of Mo<sub>2</sub>Ga<sub>2</sub>C extremely decrease,

validating the successful preparation of Mo<sub>2</sub>CT<sub>x</sub> MXenes. The shift and broaden of (002) peak also reveal the increase in the interlayer spacing and *c*-lattice parameter (*c*-LP) from 17.86 to 22 Å. Notably, over-etching can also lead to the formation of carbides (signal around 25°). Concentrated HCl can inhibit the oxidation during etching process and lower reaction temperature or dilute hydrochloric acid would reduce the efficiency and quality including oxidation of final product although with lower pressure (Figure S5, Supporting Information).

X-ray electron spectroscopy (XPS) survey spectrum of Mo<sub>2</sub>Ga<sub>2</sub>C and Mo<sub>2</sub>CT<sub>x</sub> are collected to investigate their changes of chemical compositions owing to the etching strategy. As presented in Figure 2c, the signals of Ga including Ga 2p (binding energy of 1145.2 and 1118.4 eV)<sup>[16]</sup> and Ga 3s, Ga 3p, and Ga 3d (centered at 160.3, 105.8, and 18.9 eV, respectively)<sup>[20,21]</sup> significantly decrease after HCl etching. Moreover, the appeared signals centered at 270 and 200 eV are ascribed to Cl 2s and Cl 2p, respectively, indicating the Cl-terminations on surface of prepared Mo<sub>2</sub>CT<sub>x</sub> MXenes. And the atomic percentage of Cl in the sample is around 6–8%, the atomic percentage of O is around 25–29%. In addition, the atomic ratio of Mo:Ga is 22.08:0.44 in Mo<sub>2</sub>CT<sub>x</sub> MXenes, suggesting that almost 98% of Mo<sub>2</sub>Ga<sub>2</sub>C is converted to MXenes. In short, we can suggest that fluoride-free Mo<sub>2</sub>CT<sub>x</sub> MXenes with high purity have been successfully synthesized with Cl- and oxygen-containing terminations, well agreeing with the above calculated predictions. The surface functional groups can also

be tunable by adding sources like nitrogen or sulfur during etching process.

Furthermore,  $\text{Mo}_2\text{CT}_x$  can be simply delaminated with high quality via the intercalation of TMAOH and ultrasonication as shown in Figures S6 and S7 (Supporting Information). The colloidal suspension of  $\text{Mo}_2\text{CT}_x$  flakes could also be easily aggregated with the addition of small amount of cations such as  $\text{Na}^+$  as shown in Figure S8 (Supporting Information). Owing to the high purity, easy delamination, and further gelation, the as-prepared fluoride-free  $\text{Mo}_2\text{CT}_x$  MXenes are expected to show inspiring prospect in future applications.

The morphology of  $\text{Mo}_2\text{Ga}_2\text{C}$  and  $\text{Mo}_2\text{CT}_x$  MXenes is investigated through electron microscopy as shown in Figure S9a (Supporting Information) and Figure 2d.  $\text{Mo}_2\text{Ga}_2\text{C}$  shows typical densely stacked structure with micrometer size just like the other MAX materials, but it is separately platelet-like (Figure S10, Supporting Information) which is different from others with bulk structure. After HCl-etching,  $\text{Mo}_2\text{CT}_x$  MXenes do not show obvious accordion structure like other MXenes ( $\text{Ti}_3\text{C}_2\text{T}_x$ <sup>[22]</sup> and  $\text{V}_2\text{CT}_x$ <sup>[23]</sup>), while displaying more clear layered structure with slight expanded interlayers. Based on the elemental mapping results (Figure 2e and Figure S11, Supporting Information) of single platelet, Mo, Ga, and C uniformly distribute on  $\text{Mo}_2\text{Ga}_2\text{C}$  and Mo, C, Cl, and O atoms uniformly distribute on  $\text{Mo}_2\text{CT}_x$  MXenes. The signal of Ga atoms is significantly reduced. The comparison of energy-dispersive X-ray spectroscopy (EDS) results between plenty of  $\text{Mo}_2\text{Ga}_2\text{C}$  and  $\text{Mo}_2\text{CT}_x$  MXenes (Figure S12, Supporting Information) directly confirm the successful extraction of Ga atoms. It is further

proved from the reduction of contrast between  $\text{Mo}_2\text{CT}_x$  layers and expanded layer spacing to 1.02 from 0.91 nm measured in high-resolution transmission electron microscopy (HRTEM) (Figure 2f) compared with  $\text{Mo}_2\text{Ga}_2\text{C}$  (Figure S9b, Supporting Information) which is consistent with XRD results.

### 2.3. Structure Study of $\text{Mo}_2\text{CT}_x$

Spectral measurements including high-resolution XPS and X-ray absorption fine structure (XAFS) are further performed to study the electron structure of  $\text{Mo}_2\text{CT}_x$  MXenes. High-resolution XPS of Mo 3d spectra for  $\text{Mo}_2\text{CT}_x$  are well fitted (Figure 3a) to analyze the components of Mo atoms. The two main peaks located at 229.68 and 232.84 eV are Mo 3d<sub>5/2</sub> and Mo 3d<sub>3/2</sub> associated with  $\text{T}_x\text{-Mo-C}$  species. And the binding energy of 229.68 eV is about 1.58 eV higher than the reported 228.1 eV of the Mo-C species for  $\text{Mo}_2\text{Ga}_2\text{C}$ .<sup>[20]</sup> This higher binding energy of Mo 3d<sub>5/2</sub> for  $\text{Mo}_2\text{CT}_x$  MXenes indicates the increase of Mo valence owing to the extraction of Ga and grafted terminations. While the other four peaks are ascribed to the oxidation of Mo. The Mo 3d<sub>5/2</sub> and Mo 3d<sub>3/2</sub> at 230.52 and 233.73 eV are attributed to  $\text{Mo}^{5+}$ , additionally, the two peaks centered at 231.74 eV (Mo 3d<sub>5/2</sub>) and 235.68 eV (Mo 3d<sub>3/2</sub>) are attributed to  $\text{Mo}^{6+}$  species.<sup>[13,24]</sup> The calculated percentage of  $\text{Mo}^{5+}$  and  $\text{Mo}^{6+}$  are 15.5% and 15%, respectively. C 1s spectra of  $\text{Mo}_2\text{CT}_x$  (Figure 3b) are also deconvoluted into four dominate peaks located around 283.65, 284.77, 286.03, and 289.0 eV which are in accordance with C-Mo-T<sub>x</sub>, C-C, C-Cl/C-OH, and C=O, respectively.<sup>[25]</sup>

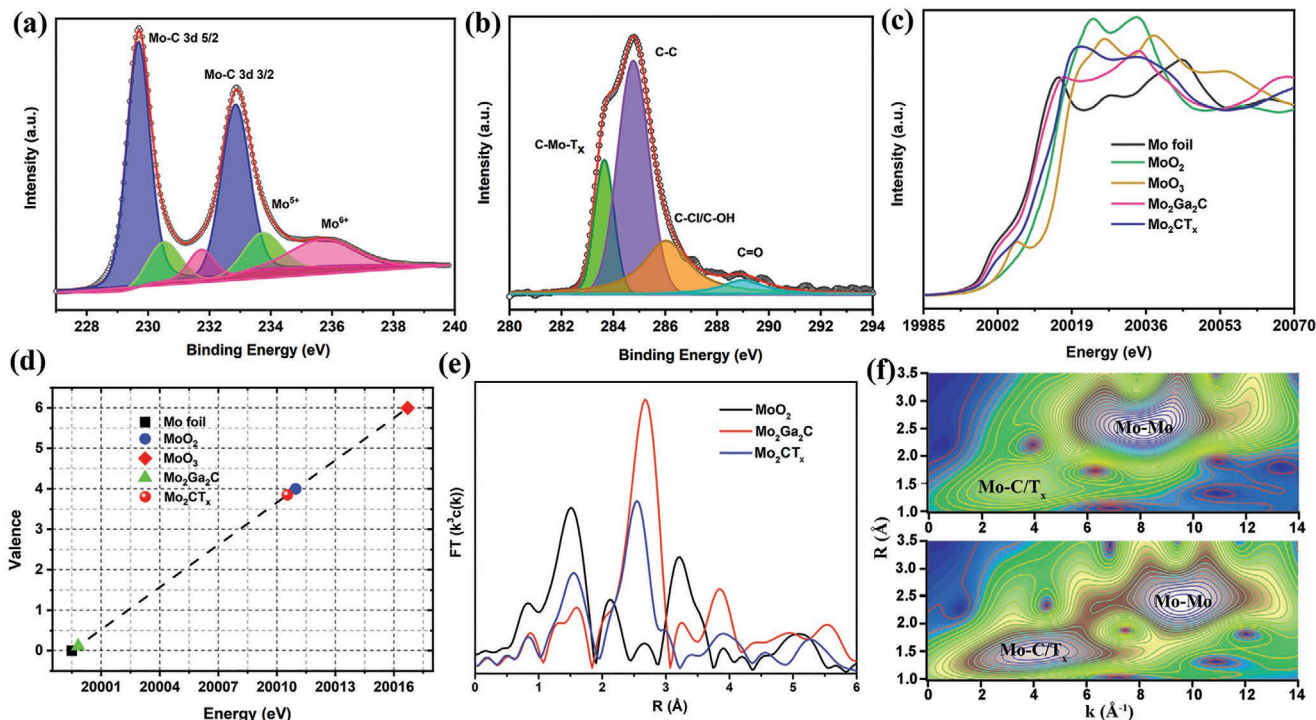


**Figure 3.** Structure characterization of  $\text{Mo}_2\text{CT}_x$  MXenes. a,b) High-resolution XPS spectrum of Mo3d and C1s for  $\text{Mo}_2\text{CT}_x$  MXenes. c) Normalized XANES spectra of Mo K-edge for Mo foil,  $\text{MoO}_2$  powder,  $\text{Mo}_2\text{Ga}_2\text{C}$  and  $\text{Mo}_2\text{CT}_x$  MXenes. d) Calculated chemical valences for Mo atom in  $\text{Mo}_2\text{Ga}_2\text{C}$  and  $\text{Mo}_2\text{CT}_x$  MXenes. e) FT-EXAFS of Mo K-edge for  $\text{MoO}_2$  powder,  $\text{Mo}_2\text{Ga}_2\text{C}$  and  $\text{Mo}_2\text{CT}_x$  MXenes. f) Wavelet transform (WT) of  $\text{Mo}_2\text{Ga}_2\text{C}$  (above) and  $\text{Mo}_2\text{CT}_x$  MXenes (below), respectively.

It indicates the possible termination of Cl groups which is further confirmed from the analysis of Cl 2p spectrum (Figure S13, Supporting Information). While the Cl 2p<sub>3/2</sub> centered at 198.97 and 200.13 eV are ascribed to Mo–Cl and C–Cl, respectively.<sup>[26]</sup> Additionally, the form of Cl functional groups in Mo<sub>2</sub>CT<sub>x</sub> MXenes is mainly Mo–Cl with a percentage of 62.75%.

Mo K-edge XAFS is further collected to study the structure of Mo<sub>2</sub>CT<sub>x</sub> MXenes. The absorption edge of Mo is obviously shifted to higher energy compared with Mo<sub>2</sub>Ga<sub>2</sub>C (Figure 3c) implying the increase of Mo valence in Mo<sub>2</sub>CT<sub>x</sub> MXenes which is in consistent with XPS results. In detail, the energy of Mo absorption edge for Mo<sub>2</sub>Ga<sub>2</sub>C is 19 999.81 eV which is very close to Mo foil (19 999.49 eV). Therefore, the valence of Mo in Mo<sub>2</sub>Ga<sub>2</sub>C is close to 0. Besides, the edge position of Mo<sub>2</sub>CT<sub>x</sub> is much higher (20 010.54 eV) and near to MoO<sub>2</sub> (20 010.97 eV) indicating the similar valence of +4. Based on the references of Mo foil, MoO<sub>2</sub>, and MoO<sub>3</sub>, we calculate the average valence of Mo in Mo<sub>2</sub>Ga<sub>2</sub>C and Mo<sub>2</sub>CT<sub>x</sub> with the results of +0.11 and +3.85, respectively (Figure 3d). The obvious increase of Mo valence is attributed to the Mo vacancy, surface oxidation of Mo with valence of +5 and +6, and the grafted anion termination including Cl- and O-containing functional groups.<sup>[14]</sup> The corresponding Fourier-transformed extended X-ray absorption fine structure (FT-EXAFS) in Figure 3e exhibits the changes of local structure of Mo including bond length and coordination number between Mo<sub>2</sub>Ga<sub>2</sub>C and Mo<sub>2</sub>CT<sub>x</sub>. The detailed results are well fitted (Figure S14, Supporting Information) and concluded in Table S3 (Supporting Information). After HCl etching, the first shell scattering of Mo–C/T<sub>x</sub> is increased and the coordination number increased to 4.81 from 3 of Mo<sub>2</sub>Ga<sub>2</sub>C. This increase is mainly attributed from the plenty of additional functional groups. Moreover, coordination number of Mo–Ga significantly decreases and the bond length of Mo–Mo (Mo–C–Mo) in Mo<sub>2</sub>CT<sub>x</sub> decrease to 2.88 from 3.03 Å of Mo<sub>2</sub>Ga<sub>2</sub>C owing to the extraction of Ga, the coordination number of Mo–Mo also decrease to 3.11 from 6.11 which attributes from the production of Mo vacancy<sup>[27]</sup> similar to the loss of Ti during the etching of Ti<sub>3</sub>AlC<sub>2</sub>.<sup>[28]</sup> Wavelet transform (WT) is used to analyze Mo

K-edge EXAFS oscillations (Figure 3f). The WT maximum at 4.1 and 9.6 Å<sup>-1</sup> for Mo<sub>2</sub>CT<sub>x</sub> can be assigned to Mo–C/T<sub>x</sub> and Mo–Mo bonds, respectively. The obvious difference of Mo–Mo bonds for Mo<sub>2</sub>CT<sub>x</sub> compared with Mo<sub>2</sub>Ga<sub>2</sub>C (8.2 Å<sup>-1</sup>) indicates the change of scattering owing to the removal of Ga. And the difference of intensity maximum of Mo–C/T<sub>x</sub> confirms the changes of surface terminations.

#### 2.4. Etching Mechanism Study of Mo<sub>2</sub>Ga<sub>2</sub>C

DFT calculation is further performed to understand the etching mechanism of Mo<sub>2</sub>Ga<sub>2</sub>C in HCl. In our simulations, HCl molecules are participated one by one at the boundaries of Mo<sub>2</sub>Ga<sub>2</sub>C, followed by complete relaxation. More than 30 configurations of HCl intercalation are taken into account and the one with lowest energy is used for the addition of next HCl molecular. According to the DFT results (Figure S15, Supporting Information), the etching process initially happens at the exposed edge sites with the spontaneous dissociation of HCl which is similar to the etching of Ti<sub>3</sub>C<sub>2</sub> by HF.<sup>[18]</sup> The extraction of Ga leads to the formation of GaCl<sub>3</sub>, and expands the grain boundary, further accelerating the penetration of Cl ions and weakening Mo–Ga bond. Moreover, resulted from the etching of aqueous HCl solution, there will be plenty of Cl-terminations and OH functional groups on the surface of Mo<sub>2</sub>C MXenes, which is important in the dissociation of MAX. The calculated binding energies of Cl and OH are about –3.28 and –2.84 eV, respectively, implying the grafting of Cl/OH groups.

To reveal the nature of bonds during the etching process, electron localization function (ELF)<sup>[29]</sup> is simulated in Figure 4, where ELF = 1 corresponds to the perfect localization, ELF = 0.5 indicates the electron gas, and ELF = 0 refers to complete delocalization. In Mo<sub>2</sub>Ga<sub>2</sub>C MAX, there is a strong covalent bond between Mo and C with a high ELF (0.72–0.76), while Mo–Ga bond is relatively weak (ELF = 0.52–0.57). For the edge bond of Mo–Ga, a smaller localized electron density (ELF ≈ 0.36) indicates the weaker bonding. Intriguingly, there is a spilled

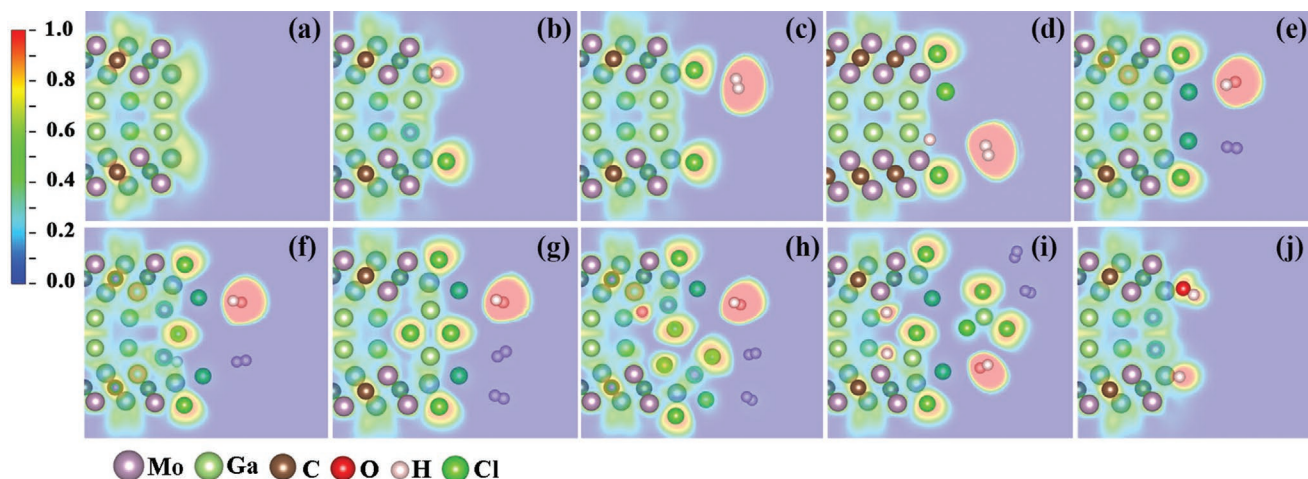


**Figure 4.** Etching process of Mo<sub>2</sub>CT<sub>x</sub> from Mo<sub>2</sub>Ga<sub>2</sub>C MAX in hydrochloric acid. a) Electron localization function plots for pristine Mo<sub>2</sub>Ga<sub>2</sub>C MAX. b–i) Electron localization function plots for etched Mo<sub>2</sub>Ga<sub>2</sub>C with the addition of 1–7 HCl, respectively. j) H<sub>2</sub>O dissociation at the edge of MAX and subsequent termination of edge Mo atoms by OH.

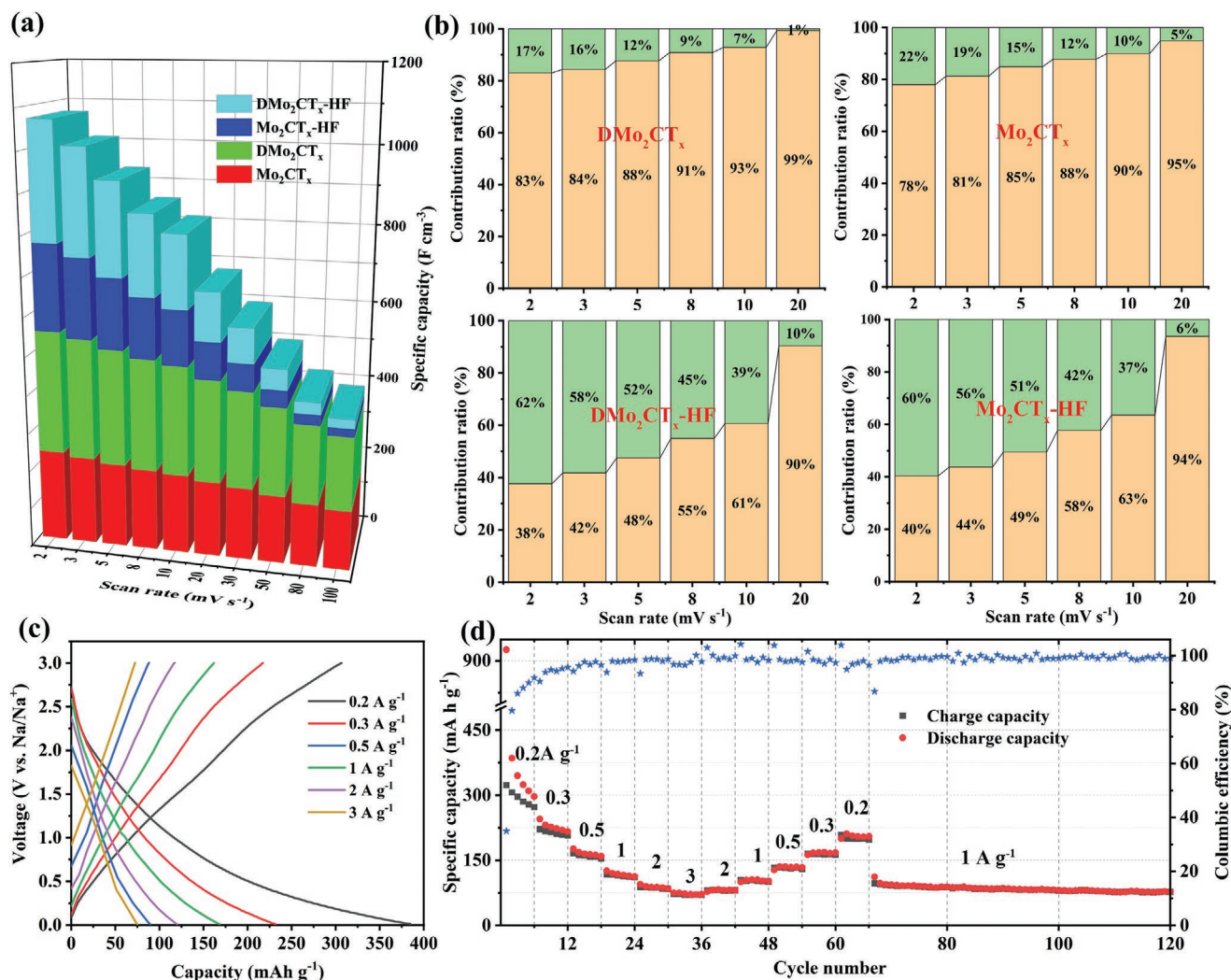


**Figure 5.** Applications of fluoride-free Mo<sub>2</sub>CT<sub>x</sub> MXenes. Supercapacitor performance in 1 M H<sub>2</sub>SO<sub>4</sub> electrolyte. a) Rate performance of different vacuum-filtered Mo<sub>2</sub>CT<sub>x</sub> films at scan rates of 2 to 100 mV s<sup>-1</sup>. b) The percentage of surface capacity (yellow) and intercalation pseudocapacitance (green) of the indicated MXenes film electrodes. Electrochemical performance as electrodes in SIBs. c) Galvanostatic charge and discharge curves cycled at different current densities. d) Rate and cyclic performance.

charge density at the edge of MAX, leading to the dissociation of HCl and H<sub>2</sub>O followed by their adsorption (Figure 4a). After HCl molecules are added one by one, robust bonds between Cl/OH and Mo are formed owing to the high localized electron (Figure 4b–j) with the evolution of H<sub>2</sub>.<sup>[22,30]</sup> Terminations of Cl/OH drastically weaken Mo–Ga bond (ELF ≈ 0.10), promoting the further extraction of interior Ga atoms.

## 2.5. Electrochemical Applications

Mo<sub>2</sub>CT<sub>x</sub> film electrodes for supercapacitors in 1 M H<sub>2</sub>SO<sub>4</sub> and 1 M Na<sub>2</sub>SO<sub>4</sub> electrolytes are studied. The reference sample is Mo<sub>2</sub>CT<sub>x</sub> prepared via traditional HF-etching method (Mo<sub>2</sub>CT<sub>x</sub>-HF, Figure S16, Supporting Information). For better comparison, samples prepared via HCl, HF, and their delaminations (DMo<sub>2</sub>CT<sub>x</sub>, DMo<sub>2</sub>CT<sub>x</sub>-HF) with little amount of CNT are fabricated into free-standing films (Figure S17, Supporting

Information). In 1 M H<sub>2</sub>SO<sub>4</sub> electrolyte, Mo<sub>2</sub>CT<sub>x</sub> MXenes prepared via HCl both in bulk or multilayer exhibit much better rate performance than that prepared in HF (Figure 5a and Figure S18, Supporting Information) mainly because of the distinction of F and Cl terminations. The difference is further investigated via electrochemical reaction kinetics based on the equation  $i(V) = k_1v + k_2v^{0.5}$ , where the current ( $i$ ) at a potential ( $V$ ) can be divided into surface capacitive effect ( $k_1v$ ) and diffusion-limited component from intercalation pseudocapacitance ( $k_2v^{0.5}$ ).<sup>[31]</sup> As shown in Figure 5b, surface capacitance behavior of both DMo<sub>2</sub>CT<sub>x</sub> and Mo<sub>2</sub>CT<sub>x</sub> prepared via HCl is always the dominant contribution, resulting in excellent rate performance. However, for MXenes of DMo<sub>2</sub>CT<sub>x</sub>-HF and Mo<sub>2</sub>CT<sub>x</sub>-HF, the intercalation pseudocapacitance under low scan rates is the dominant contribution which will rapidly diminish at higher scan rates over 20 mV s<sup>-1</sup>, leading to poor rate property. However, both Mo<sub>2</sub>CT<sub>x</sub> and Mo<sub>2</sub>CT<sub>x</sub>-HF exhibit similar storage mechanism with major contribution from surface capacitance

in 1 M Na<sub>2</sub>SO<sub>4</sub> electrolyte (Figure S19, Supporting Information). The Mo<sub>2</sub>CT<sub>x</sub> electrode also exhibits excellent cyclic stability under 5 A g<sup>-1</sup>. During the cycling process, the specific capacity gradually increases. And there is about 16.1% of capacity increase after 10 000 cycles compared with the initial capacity. This increase mainly resulted from the replacement of Cl by O-containing groups owing to the higher binding energy calculated from DFT which needs further investigation on experiments. Based on the above research, the surface terminations on Mo<sub>2</sub>CT<sub>x</sub> formed during HCl hydrothermal etching process show significant effect on the energy storage mechanism of supercapacitors in different electrolytes.

The electrochemical property of Mo<sub>2</sub>CT<sub>x</sub> electrodes in sodium ion batteries (SIBs) is further measured. The galvanostatic charge and discharge (GCD) curves under different current densities are shown in Figure 5c and the cell can work in the voltage window of 0.01–3 V. Combined with the rate property as shown in Figure 5d, Mo<sub>2</sub>CT<sub>x</sub> electrode can deliver a discharge capacity of 385.2 mA h g<sup>-1</sup> after the first cycle of (de)lithiation at 0.2 A g<sup>-1</sup>. And a reversible specific capacity of 204.8 mA h g<sup>-1</sup> at 0.2 A g<sup>-1</sup> after 65 cycles of rate testing is observed. The clear deterioration is because of the formation of solid electrolyte interphase (SEI) or the irreversible reaction of Na with the surface terminations during the initial cycles which needs further investigation.<sup>[32]</sup> However, at 3 A g<sup>-1</sup>, there is still a capacity of 72.3 mA h g<sup>-1</sup> retained. After rate program, a reversible capacity of 96.6 mA h g<sup>-1</sup> under 1 A g<sup>-1</sup> is remained and exhibiting a stable cycling performance with high columbic efficiency. Moreover, electrochemical impedance spectroscopy (EIS, Figure S20, Supporting Information) shows a low equivalent series resistance (R<sub>s</sub>) of 5.6 Ω and charge transfer resistance (R<sub>ct</sub>) of 41.6 Ω indicating the good conductivity of Mo<sub>2</sub>CT<sub>x</sub>.

### 3. Conclusion

Controllable HCl-hydrothermal etching strategy for MXenes is developed based on DFT calculation of the feasibility and optimal etching conditions of MAX phases (A = Al, Ga). Fluoride-free Mo<sub>2</sub>CT<sub>x</sub> MXenes with high quality are realized and exhibits modulated energy storage mechanism in energy storage applications. By successfully extending the strategy to diverse MAX systems, this research should hold great promise for the diversification of MAX and MXenes analogues and the activation/stabilization of ideal surface for extensive applications.

### 4. Experimental Section

**First-Principles Calculations:** First-principles calculations are performed by using DFT<sup>[33]</sup> within project augmented wave method (PAW)<sup>[34]</sup> which is implemented in the Vienna Ab initio Simulation Package (VASP).<sup>[35]</sup> Perdue–Burke–Ernzerhof (PBE)<sup>[36]</sup> version of the generalized gradient approximation (GGA) was performed to deal with exchange and correlation energy. The Brillouin zone was sampled by using 3 × 3 × 1 for surface and 7 × 7 × 2 for bulk, respectively, based on Monkhorst–Pack k-point mesh. A plane-wave cutoff energy of 450 eV is efficient to guarantee the convergence of the total energy. The atoms in the surface configuration at leftmost are fixed and others are completely relaxed with

force below 0.01 eV Å<sup>-1</sup>. Moreover, 20 Å vacuum is considered to avoid spurious interaction. The chemical potential of A (A = Al, Ga) in ACI<sub>3</sub> and MAX can be expressed as follows<sup>[18]</sup>

$$E(\text{ACI}_3) = \mu_A + 3\mu_{\text{Cl}} \quad (1)$$

$$E(\text{MAX}) = 2\mu_M + \mu_A + \mu_X \quad (2)$$

based on Equations (1) and (2), the relation of  $\mu_A(\text{ACI}_3) < \mu_A(\text{MAX})$  can be defined as

$$E(\text{ACI}_3) - 3\mu_{\text{Cl}} < E(\text{MAX}) - \mu_M - \mu_X \quad (3)$$

where  $\mu_M$  and  $\mu_X$  are referenced to the chemical potential of M and X in bulk M and graphite, respectively. The chemical potential of Cl in solution considering as a reservoir relies on practical environment which is treated as a variable.  $\mu_{\text{Cl}} = E_{\text{HCl}} - \frac{1}{2}\mu_{\text{H}}[\text{H}_2]$ , owing to dissociation of HCl into H<sub>2</sub> and Cl<sub>2</sub>. The chemical potential of H is the total energy of isolated H<sub>2</sub> molecules.

**Synthesis of Mo<sub>2</sub>Ga<sub>2</sub>C MAX:** Mo<sub>2</sub>Ga<sub>2</sub>C flakes were synthesized via a modified two-stage vacuum sintering process. Briefly, 3 g commercial Mo<sub>2</sub>C powder (around 325 mesh, 99.5%, metals basis) and Ga (99.99%, metal basis) was uniformly mixed in a mortar at 60 °C with a molar ratio of 1:8 for 1 h. Then, the mixture was transferred into a glass tube and vacuumed by a mechanical pump. The glass tube was further sealed under a stable vacuuming state and annealed in a muffle furnace for 3 d at 850 °C. After the natural cooling, the mixture was homogeneously grinded in a mortar at 60 °C again. And the following procedure was the same with the first stage except the duration of annealing time was 2 d. To remove the extra Ga, the mixture was immersed in 50 mL concentrated hydrochloric acid under stirring for one night at room temperature. After washed several times by deionized water until the pH was nearly 7 and freeze-drying for 1 d, the Mo<sub>2</sub>Ga<sub>2</sub>C flakes were obtained.

**Synthesis of Mo<sub>2</sub>CT<sub>x</sub> MXenes and Its Delamination:** Fluoride-free Mo<sub>2</sub>CT<sub>x</sub> MXenes were prepared through a hydrothermal etching process with concentrate HCl. 200 mg of the obtained Mo<sub>2</sub>Ga<sub>2</sub>C and 20 mL HCl (12 M) was put into a 50 mL autoclave with a Teflon liner. Afterward, the autoclave was placed into an oven for 5 d at 120 and 140 °C. After cooling to room temperature, the samples were washed several times with deionized water and ethanol. Then, fluoride-free Mo<sub>2</sub>CT<sub>x</sub> MXenes were obtained after freeze-drying for 1 d. For the delamination of Mo<sub>2</sub>CT<sub>x</sub> MXenes (DMo<sub>2</sub>CT<sub>x</sub>), 100 mg Mo<sub>2</sub>CT<sub>x</sub> was transferred into 3 mL 25% tetramethylammonium hydroxide (TMAOH) solution and stirred for 3 h at room temperature. After the centrifugation and washed two times with deionized water, the sediment was dispersed in 40 mL water by ultrasonication for 1 h under 10 °C water cooling. Finally, the suspension of delaminated Mo<sub>2</sub>CT<sub>x</sub> flakes was obtained after centrifugation under 3000 rpm for 20 min. Fluorine-terminated Mo<sub>2</sub>CT<sub>x</sub> MXenes as reference samples were also prepared via HF-etching strategy (Mo<sub>2</sub>CT<sub>x</sub>-HF). 200 mg Mo<sub>2</sub>Ga<sub>2</sub>C was immersed in 20 mL hydrofluoric acid for 5 d at 60 °C. Sample was washed with deionized water and centrifugation for several times until the pH was nearly 7. Then Mo<sub>2</sub>CT<sub>x</sub>-HF powder was obtained after freeze-drying for 1 d. The delamination of Mo<sub>2</sub>CT<sub>x</sub>-HF (DMo<sub>2</sub>CT<sub>x</sub>-HF) followed the same procedures of DMo<sub>2</sub>CT<sub>x</sub>.

**Electrochemical Measurements: Supercapacitors:** The electrochemical characterization of Mo<sub>2</sub>CT<sub>x</sub> MXenes in supercapacitor was achieved in a three-electrode testing system. The working electrode of Mo<sub>2</sub>CT<sub>x</sub> MXenes and CNT film was prepared by using vacuum-assisted filtration method. Mo<sub>2</sub>CT<sub>x</sub> was mixed with PVP-grafted CNT by ultrasonication for 1 h under 10 °C water cooling with the mass ratio about 25:1. The solution was filtered through a mixed cellulose membrane with vacuum filtration. Then the standing film was obtained after freeze-drying and peeling off from the filter membrane. In the three-electrode testing system, Ag/AgCl (3 M KCl), Pt foil, and 1 M H<sub>2</sub>SO<sub>4</sub> (1 M Na<sub>2</sub>SO<sub>4</sub>) were used as reference electrode, counter electrode, and electrolyte, respectively. The prepared

Mo<sub>2</sub>CT<sub>x</sub> and CNT films were used as working electrode directly. The performance testing was achieved on a CHI760E working station. In more detail, the cyclic voltammetry (CV) curves were collected under different voltage scan rates in the voltage window of −0.1 to 0.4 V (vs Ag/AgCl) in 1 M H<sub>2</sub>SO<sub>4</sub> and −0.5 to 0.1 V in 1 M Na<sub>2</sub>SO<sub>4</sub>. EIS was tested on an electrochemical workstation (CHI760E) over the frequency range of 10<sup>6</sup>–0.02 Hz with 5 mV AC oscillation amplitude.

**Electrochemical Measurements: Sodium-Ion Batteries:** The electrochemical test of Mo<sub>2</sub>CT<sub>x</sub> MXenes electrodes in SIBs was carried out in CR2032 coin-type cells. Mo<sub>2</sub>CT<sub>x</sub> MXenes, carbon black, and polyvinylidene fluoride (PVDF) were firstly mixed and grinded into homogeneous slurry in *N*-methyl-2-pyrrolidone (NMP) with a mass ratio of 7:2:1. The slurry was then spread on a copper substrate with a coater. After pre-dried in an oven for 1 h under 70 °C, it was transferred in another vacuum oven for 12 h under 100 °C. The electrode with a diameter of 16 mm was finally obtained by using a punching machine and assembled into coin-type cell with sodium tablet as counter electrode and 1 M NaClO<sub>4</sub> in (EC:DMC, 1:1) as electrolyte. The assembling procedure was carried out in an argon-filled glovebox. Rate performance of the SIBs cell was collected on a Land CT2001A testing system at room temperature in the working voltage window of 0.01–3 V. Moreover, the EIS testing was carried out with the same procedure as supercapacitors.

**Material Characterization:** XRD patterns were collected on a D8-Advance power diffractometer equipped with Cu K $\alpha$  radiation ( $\lambda = 1.54178 \text{ \AA}$ ) and a step scan of 0.02°. XPS was recorded on electron energy-dispersive spectroscopy (ESCALAB 250). Scanning electron microscopy (SEM) images and elemental mapping results were obtained on a cold field emission scanning electron microscope (SU8220). TEM images and HRTEM images were collected on a transmission electron microscope (JEOL JEM2010). Atomic force microscopy (AFM) data were collected on a scanning probe microscope (Multimode V). The etching efficiency of Mo<sub>2</sub>CT<sub>x</sub> was calculated from XPS and plasma atomic emission spectrograph (Optima 7300 DV) results. A plasma atomic emission spectrograph was used to detect the atomic concentration of Mo and Ga in dilute chloroazotic acid. The Mo K-edge XAFS measurements were realized in the transmission mode at the beamline 14W1 in Shanghai Synchrotron Radiation Facility (SSRF). The X-ray was monochromatized by a double-crystal Si(111) monochromator, and the energy was calibrated using a molybdenum metal foil for Mo K-edge. XAFS data were analyzed with the WinXAS3.1 program.<sup>[37]</sup> Theoretical amplitudes and phase-shift functions of Mo–C–T<sub>x</sub> and Mo–Mo were calculated with the FEFF8.2 code<sup>[38]</sup> using the crystal structural parameters of the MoO<sub>2</sub> foil.

## Supporting Information

Supporting Information is available from the Wiley Online Library or from the author.

## Acknowledgements

C.W. and H.S. contributed equally to this work. This work was financially supported in part by National Key R&D Program of China (2020YFA0405800, 2017YFA0303500), NSFC (U1932201, 21727801), International Partnership Program of CAS (211134KYSB20190063), CAS Collaborative Innovation Program of Hefei Science Center (2019HSC-CIP002), National Postdoctoral Program for Innovative Talents (BX20190315), Anhui Provincial Natural Science Foundation (2008085QA28), and the Fundamental Research Funds for the Central Universities (Grant No. WK2310000088). L.S. acknowledges the support from Key Laboratory of Advanced Energy Materials Chemistry (Ministry of Education), Nankai University (111 project, B12015). The authors thank the Shanghai synchrotron Radiation Facility (14W1, SSRF), the Beijing Synchrotron Radiation Facility (1W1B and 4B9A, BSRF), the Hefei

Synchrotron Radiation Facility (MCD-A and MCD-B Soochow Beamline for Energy Materials, Photoemission and Catalysis/Surface Science at NSRL), and the USTC Center for Micro and Nanoscale Research and Fabrication for help in characterizations.

## Conflict of Interest

The authors declare no conflict of interest.

## Data Availability Statement

Research data are not shared.

## Keywords

energy storage, fluoride-free MXenes, high electrochemical performance, hydrothermal etching, MXenes, supercapacitors

Received: February 5, 2021

Revised: March 22, 2021

Published online:

- [1] Y. F. Dong, H. D. Shi, Z. S. Wu, *Adv. Funct. Mater.* **2020**, *30*, 2000706.
- [2] C. D. Wang, S. M. Chen, L. Song, *Adv. Funct. Mater.* **2020**, *30*, 2000869.
- [3] L. Verger, V. Natu, M. Carey, M. W. Barsoum, *Trends Chem.* **2019**, *1*, 656.
- [4] M. Ghidui, M. R. Lukatskaya, M. Q. Zhao, Y. Gogotsi, M. W. Barsoum, *Nature* **2014**, *516*, 78.
- [5] J. L. Hart, K. Hantanasirisakul, A. C. Lang, B. Anasori, D. Pinto, Y. Pivak, J. T. van Omme, S. J. May, Y. Gogotsi, M. L. Taheri, *Nat. Commun.* **2019**, *10*, 522.
- [6] H. Yu, Y. Wang, Y. Jing, J. Ma, C. F. Du, Q. Yan, *Small* **2019**, *15*, 1901503.
- [7] a) C. Eames, M. S. Islam, *J. Am. Chem. Soc.* **2014**, *136*, 16270; b) T. Schultz, N. C. Frey, K. Hantanasirisakul, S. Park, S. J. May, V. B. Shenoy, Y. Gogotsi, N. Koch, *Chem. Mater.* **2019**, *31*, 6590.
- [8] a) X. Xie, Y. Xue, L. Li, S. Chen, Y. Nie, W. Ding, Z. Wei, *Nanoscale* **2014**, *6*, 11035; b) B. Zhang, J. Zhu, P. Shi, W. Wu, F. Wang, *Ceram. Int.* **2019**, *45*, 8395; c) G. Li, L. Tan, Y. Zhang, B. Wu, L. Li, *Langmuir* **2017**, *33*, 9000; d) T. Li, L. Yao, Q. Liu, J. Gu, R. Luo, J. Li, X. Yan, W. Wang, P. Liu, B. Chen, W. Zhang, W. Abbas, R. Naz, D. Zhang, *Angew. Chem., Int. Ed. Engl.* **2018**, *57*, 6115.
- [9] a) M. R. Lukatskaya, J. Halim, B. Dyatkin, M. Naguib, Y. S. Buranova, M. W. Barsoum, Y. Gogotsi, *Angew. Chem., Int. Ed. Engl.* **2014**, *53*, 4877; b) W. Sun, S. A. Shah, Y. Chen, Z. Tan, H. Gao, T. Habib, M. Radovic, M. J. Green, *J. Mater. Chem. A* **2017**, *5*, 21663.
- [10] a) M. Li, J. Lu, K. Luo, Y. Li, K. Chang, K. Chen, J. Zhou, J. Rosen, L. Hultman, P. Eklund, P. O. A. Persson, S. Du, Z. Chai, Z. Huang, Q. Huang, *J. Am. Chem. Soc.* **2019**, *141*, 4730; b) V. Kamysbayev, A. S. Filatov, H. Hu, X. Rui, F. Lagunas, D. Wang, R. F. Klie, D. V. Talapin, *Science* **2020**, *369*, 979; c) Y. Li, H. Shao, Z. Lin, J. Lu, L. Liu, B. Duployer, P. O. A. Persson, P. Eklund, L. Hultman, M. Li, K. Chen, X. H. Zha, S. Du, P. Rozier, Z. Chai, E. Raymundo-Pinero, P. L. Taberna, P. Simon, Q. Huang, *Nat. Mater.* **2020**, *19*, 894.
- [11] Q. Sun, Y. Dai, Y. Ma, T. Jing, W. Wei, B. Huang, *J. Phys. Chem. Lett.* **2016**, *7*, 937.
- [12] S. Y. Pang, Y. T. Wong, S. Yuan, Y. Liu, M. K. Tsang, Z. Yang, H. Huang, W. T. Wong, J. Hao, *J. Am. Chem. Soc.* **2019**, *141*, 9610.



- [13] J. Halim, S. Kota, M. R. Lukatskaya, M. Naguib, M.-Q. Zhao, E. J. Moon, J. Pitcock, J. Nanda, S. J. May, Y. Gogotsi, M. W. Barsoum, *Adv. Funct. Mater.* **2016**, *26*, 3118.
- [14] E. B. Deeva, A. Kurlov, P. M. Abdala, D. Lebedev, S. M. Kim, C. P. Gordon, A. Tsoukalou, A. Fedorov, C. R. Müller, *Chem. Mater.* **2019**, *31*, 4505.
- [15] Y. T. Guo, S. Jin, L. B. Wang, P. G. He, Q. K. Hu, L. Z. Fan, A. G. Zhou, *Ceram. Int.* **2020**, *46*, 19550.
- [16] K. R. G. Lim, A. D. Handoko, L. R. Johnson, X. Meng, M. Lin, G. S. Subramanian, B. Anasori, Y. Gogotsi, A. Vojvodic, Z. W. Seh, *ACS Nano* **2020**, *14*, 16140.
- [17] A. Vojvodic, A. J. Medford, F. Studt, F. Abild-Pedersen, T. S. Khan, T. Bligaard, J. K. Nørskov, *Chem. Phys. Lett.* **2014**, *598*, 108.
- [18] P. Srivastava, A. Mishra, H. Mizuseki, K. R. Lee, A. K. Singh, *ACS Appl. Mater. Interfaces* **2016**, *8*, 24256.
- [19] C. Hu, C. C. Lai, Q. Tao, J. Lu, J. Halim, L. Sun, J. Zhang, J. Yang, B. Anasori, J. Wang, Y. Sakka, L. Hultman, P. Eklund, J. Rosen, M. W. Barsoum, *Chem. Commun.* **2015**, *51*, 6560.
- [20] C. C. Lai, R. Meshkian, M. Dahlgvist, J. Lu, L. A. Naslund, O. Rivin, E. N. Caspi, O. Ozeri, L. Hultman, P. Eklund, M. W. Barsoum, J. Rosen, *Acta Mater.* **2015**, *99*, 157.
- [21] J. Mei, G. A. Ayoko, C. F. Hu, J. M. Bell, Z. Q. Sun, *Sustainable Mater. Technol.* **2020**, *25*, e00156.
- [22] M. Naguib, M. Kurtoglu, V. Presser, J. Lu, J. Niu, M. Heon, L. Hultman, Y. Gogotsi, M. W. Barsoum, *Adv. Mater.* **2011**, *23*, 4248.
- [23] C. Wang, H. Xie, S. Chen, B. Ge, D. Liu, C. Wu, W. Xu, W. Chu, G. Babu, P. M. Ajayan, L. Song, *Adv. Mater.* **2018**, *30*, 1802525.
- [24] Z. W. Seh, K. D. Fredrickson, B. Anasori, J. Kibsgaard, A. L. Strickler, M. R. Lukatskaya, Y. Gogotsi, T. F. Jaramillo, A. Vojvodic, *ACS Energy Lett.* **2016**, *1*, 589.
- [25] a) W. Feng, R. Wang, Y. Zhou, L. Ding, X. Gao, B. Zhou, P. Hu, Y. Chen, *Adv. Funct. Mater.* **2019**, *29*, 1901942; b) L. J. Wan, Y. Q. Tang, L. Chen, K. Wang, J. Q. Zhang, Y. Gao, J. Y. Lee, T. Lu, X. Xu, J. B. Li, Y. H. Zheng, L. K. Pan, *Chem. Eng. J.* **2021**, *410*, 128349.
- [26] a) J. M. Gonzalez-Dominguez, P. Castell, S. Bospin-Gascon, A. Anson-Casaos, A. M. Diez-Pascual, M. A. Gomez-Fatou, A. M. Benito, W. K. Maser, M. T. Martinez, *J. Mater. Chem.* **2012**, *22*, 21285; b) X. W. Zhang, F. Meng, S. Mao, Q. Ding, M. J. Shearer, M. S. Faber, J. H. Chen, R. J. Hamers, S. Jin, *Energy Environ. Sci.* **2015**, *8*, 862; c) K. P. Wang, Y. C. Zhang, X. Zhang, L. Shen, *SN Appl. Sci.* **2019**, *1*, 157.
- [27] W. Peng, M. Luo, X. D. Xu, K. Jiang, M. Peng, D. C. Chen, T. S. Chan, Y. W. Tan, *Adv. Energy Mater.* **2020**, *10*, 2001364.
- [28] D. Zhao, Z. Chen, W. Yang, S. Liu, X. Zhang, Y. Yu, W. C. Cheong, L. Zheng, F. Ren, G. Ying, X. Cao, D. Wang, Q. Peng, G. Wang, C. Chen, *J. Am. Chem. Soc.* **2019**, *141*, 4086.
- [29] A. D. Becke, K. E. Edgecombe, *J. Chem. Phys.* **1990**, *92*, 5397.
- [30] C. Ling, L. Shi, Y. Ouyang, Q. Chen, J. Wang, *Adv. Sci.* **2016**, *3*, 1600180.
- [31] J. Li, X. T. Yuan, C. Lin, Y. Q. Yang, L. Xu, X. Du, J. L. Xie, J. H. Lin, J. L. Sun, *Adv. Energy Mater.* **2017**, *7*, 1602725.
- [32] M. Naguib, J. Halim, J. Lu, K. M. Cook, L. Hultman, Y. Gogotsi, M. W. Barsoum, *J. Am. Chem. Soc.* **2013**, *135*, 15966.
- [33] W. Kohn, L. J. Sham, *Phys. Rev.* **1965**, *140*, A1133.
- [34] P. E. Blochl, *Phys. Rev. B: Condens. Matter.* **1994**, *50*, 17953.
- [35] G. Kresse, J. Furthmuller, *Phys. Rev. B: Condens. Matter.* **1996**, *54*, 11169.
- [36] J. P. Perdew, K. Burke, M. Ernzerhof, *Phys. Rev. Lett.* **1996**, *77*, 3865.
- [37] T. Ressler, *J. Synchrotron Radiat.* **1998**, *5*, 118.
- [38] A. L. Ankudinov, B. Ravel, J. J. Rehr, S. D. Conradson, *Phys. Rev. B* **1998**, *58*, 7565.